Characterization of the microstructure, strain rate-dependent material and fracture toughness behavior of a high strength $Fe_{85}Cr_4Mo_{4.9}V_{2.1}W_{2.7}C_{1.4}$ steel

Markus Rüssel[1a], Stefan Martin[2b], Lutz Krüger[3c], Wolfgang Kreuzer[4d]

[1] Faculty of Materials Science and Technology, Institute of Materials Engineering, TU Bergakademie Freiberg, Gustav-Zeuner-Str. 5, 09599 Freiberg, Germany

[2] Faculty of Materials Science and Technology, Institute of Materials Science, TU Bergakademie Freiberg, Gustav-Zeuner-Str. 5, 09599 Freiberg, Germany

[3] Bundeswehr Research Institute for Materials, Fuels and Lubricants (WIWeB), Institutsweg 1, 85435 Erding, Germany

[1a] Markus.Ruessel@iwt.tu-freiberg.de, [2b] Stefan.Martin@iww.tu-freiberg.de, [3c] Krueger@ww.tu-freiberg.de, [4d] WolfgangKreuzer@bwb.org

Keywords: Tool steel fracture toughness, 8-point bending, Strain rate, Rapid solidification technique.

Abstract

Using a rapid solidification technique, a $Fe_{85}Cr_4Mo_{4.9}V_{2.1}W_{2.7}C_{1.4}$ (weight percent) high-speed tool steel was processed out of pure elements. Microstructural examinations of the base material were conducted with the objective of characterizing the material comprehensively. These observations revealed α'-martensite, retained austenite and complex carbides. Furthermore, strength, deformation and fracture toughness behavior was investigated. For a strain rate range from 10^{-3} s^{-1} to 10^{3} s^{-1}, the strain rate-dependent material behavior under compressive loading was examined with the aim of understanding the inherent processes during deformation. In addition, fracture toughness tests were conducted at room temperature and -40°C to determine the linear-elastic plane-strain fracture toughness K_{Ic}. Due to the difficulty of generating fatigue precracks in brittle materials, the fatigue precracking method of 8-point-bending was used, providing stable crack propagation. With this 8-point bending device, a fatigue precrack was successfully formed at a minimum-to-maximum stress ratio of R = -1 with a modified chevron-notch. The results revealed that, in comparison to other commercially available tool steels, the alloy examined exhibits relatively high fracture toughness K_{Ic}. Examinations of the influence of notch-tip radius on notch fracture toughness K_A exhibit a linear correlation between K_A and the square root of the notch root radius ρ. However, this linear correlation breaks down at a certain notch radius. Hence, the assumption was made that the critical

notch tip radius is approximately 90µm. Results from dynamic fracture toughness K_{Id} tests on a pendulum impact testing machine were compared with the static fracture toughness K_{Ic}.

Introduction

Tool steels are the most important materials for applications like cutting or drilling because of their high hardness, wear resistance and toughness. Apart from strength, it is essential to consider fracture toughness and material behavior under compressive loading as a function of strain rate, especially for design calculations of tools. Examinations regarding the strain rate-dependent material behavior of high strength alloys were performed by, for example, [1–3]. The fracture toughness K_{Ic} defines the material resistance against instable crack propagation and provides the only toughness value for the structural integrity assessment of components which contain defects. This importance is reflected in numerous fracture mechanical examinations of tool steels in the literature. The fracture toughness of tool steels is mainly determined by the heat-treatment process (hardening plus tempering temperatures) [4,5]. Typical influencing factors of the fracture toughness of tool steels are the matrix ductility and phase fraction of retained austenite and carbides, as well as the grain size [6–9]. No significant differences were found between different manufacturing conditions like conventionally wrought and powder-metallurgically produced tool steels [10]. However, less is known about the loading rate dependency on their mechanical properties.
The purpose of this research is to investigate the strain rate-dependent material behavior under compressive loading and to determine the linear-elastic plane-strain fracture toughness at low and high loading rates, (K_{Ic}) and (K_{Id}), respectively. Furthermore, the influences of temperature and notch tip radius on fracture toughness measurements were examined.

Experimental

The high strength $Fe_{85}Cr_4Mo_{4.9}V_{2.1}W_{2.7}C_{1.4}$ steel was produced in an induction furnace by melting only pure elements (minimum purity 99.99%) in an argon atmosphere and casting the melt into a copper ingot mould (dimension 14x20x120mm). In the ingot, the material solidified under a high cooling rate of at least 10K/s. For characterization of the material behavior, comprehensive examinations including optical microscopy (OM), scanning electron microscopy (SEM), X-ray diffraction analysis (XRD) and electron backscatter diffraction (EBSD) were carried out.

The strain rate-dependent material behavior under compressive loading was examined for a strain rate range from 10^{-3} s^{-1} to 10^{3} s^{-1}. Therefore, up to strain rates of 10^{0} s^{-1}, a servo-hydraulic testing machine MTS 810 was used, while an instrumented drop-weight test setup (10^{2} s^{-1}) and a Split-Hopkinson-Pressure-Bar (10^{3} s^{-1}) were used for higher strain rates. To correlate the material behavior with the microstructure, interrupted compression tests at different strains and strain rates were performed.

The determination of the linear-elastic plane-strain fracture toughness behavior was carried out in accordance with the ASTM specification E399-08 [11] utilizing Single Edge Notched Bending (SENB) specimens (width W=20mm, thickness B=14mm, length L=120mm). Generally, fatigue precracking of materials is carried out at a minimum-to-maximum stress ratio of R=0.1 using a three-point-bending device. Due to unstable crack propagation after a few loading cycles at R=0.1 with the three-point-bending device, an alternative precracking procedure was developed. In this research, fatigue precracking was carried out using an 8-point-bending device in accordance with

ISO 12108 [12] at a minimum-to-maximum stress ratio of R=-1. Fig.1 illustrates the 8-point-bending device and an example of a generated fatigue precrack.

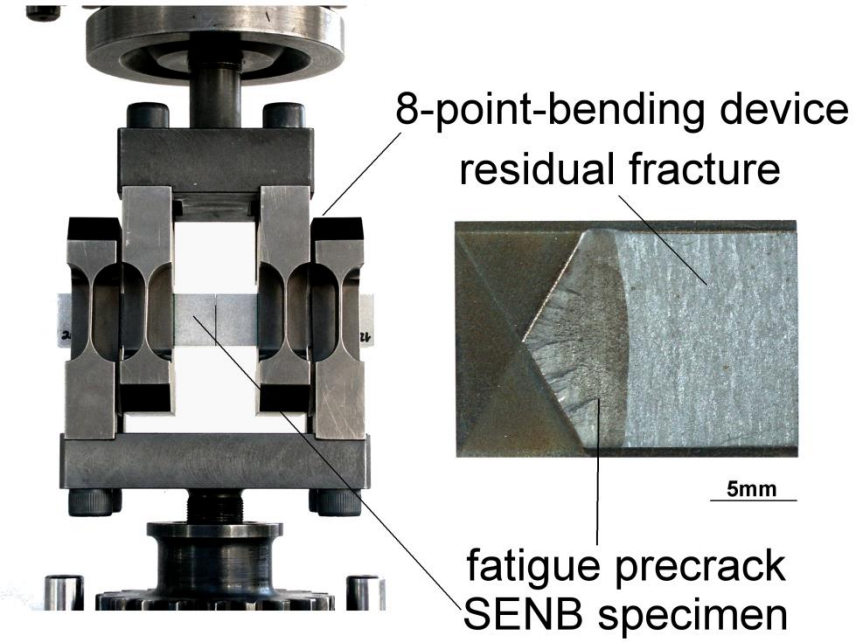

Fig.1. 8-point-bending device according to ISO 12108 [12] and an example of a generated fatigue precrack at R=-1**.**

The cyclical stress intensity factor ΔK was calculated according to a formula from Murakami [13] as follows:

$$\Delta K = \frac{3 \cdot \Delta F \cdot l}{BW^2} \cdot \sqrt{\pi \cdot a} \cdot f\left(\frac{a}{W}\right) \tag{1}$$

with the geometric factor f:

$$f\left(\frac{a}{W}\right) = 1{,}122 - 1{,}121\left(\frac{a}{W}\right) + 3{,}740\left(\frac{a}{W}\right)^2 + 3{,}873\left(\frac{a}{W}\right)^3 - 19{,}05\left(\frac{a}{W}\right)^4 + 22{,}55\left(\frac{a}{W}\right)^5 . \tag{2}$$

In equation (1) ΔF is the force, B is the thickness and W the width of the sample, while *a* is the crack length. A continuous 10% reduction of ΔK from one load level to another ensured a small plastic zone size in front of the fatigue crack tip. Crack initiation was started at a ΔK value of 18MPa√m (K_{min} = 9MPa√m, K_{max} = 9MPa√m).

For the examination of the influence of notch-tip radius on linear-elastic plane-strain fracture toughness, samples with different notch tip radii (0.035mm, 0.09mm, 0.17mm, 0.5mm and 1mm) were machined by electrical discharge machining (EDM) up to an *a/W* ratio of 0.5. A stress-intensity factor rate $\dot{K}$ of approximately 0.7MPa√m/s was chosen for the fracture toughness K_{Ic} and notch fracture toughness K_A tests.

Furthermore, dynamic fracture toughness K_{Id} tests were realized on a pendulum impact testing machine Psd300 with SENB samples of the dimensions 10x10x55mm³ ($\dot{K} \sim 10^4$ MPa√m/s).

Results and discussion

Material characterization

The as-cast solidification microstructure shows a pronounced dendritic structure with a coherent carbide network over the cross section of the cast plate. XRD data reveals the phase's martensite (body-centered cubic - bcc; phase fraction: 70.6%), retained austenite (face-centered cubic - fcc; phase fraction: 16.1%) and fcc vanadium carbide (VC) as well as hexagonal molybdenum carbide (Mo_2C), respectively. However, XRD in combination with EPMA showed that VC and Mo_2C did not occur in a pure form, but rather as complex carbides of the MC and M_2C form.
Fig.2 displays an EBSD phase map of the initial microstructure. The aforementioned phases were indexed. Based on a simultaneously executed EDS-analysis and due to topographical differences, the distinction between the two fcc phases (retained austenite and vanadium carbide) was made.

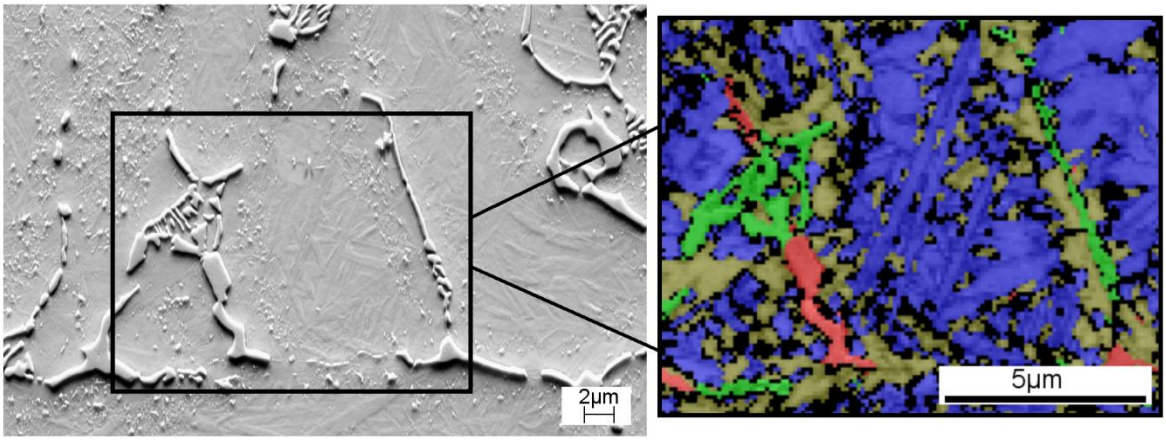

Fig.2: EBSD phase map of the initial as-cast solidification microstructure revealing bcc martensite (blue), fcc retained austenite (olive), fcc vanadium carbide (red) as well as hexagonal molybdenum carbide (green); black: not indexed.

Compressive stress-strain behavior and evolution of the microstructure

An extensive examination of the compressive stress-strain behavior of the alloy studied as well as the experimental results of the microstructural evolution is presented in [14]. Only the main facts are presented at this point.
The alloy possesses high yield strength and flow stresses as well as an ultimate compression strength of approximately 4800MPa at a deformability of 15% (strain rate: $10^{-3}s^{-1}$). The material exhibits moderate strain rate sensitivity (Fig.3a). From the microstructural point of view, a strain-induced transformation of retained austenite to martensite, so called **TR**ansformation-**I**nduced **P**lasticity (the **TRIP**-effect), was detected. Increasing deformation caused lower crystallite sizes. Due to the partitioning process of the crystallites in combination with incrementally-formed martensitic boundaries, the mean free dislocation paths are reduced, resulting in dislocation pile-ups and higher microstrains. This progressive partitioning process might be an explanation for the high compressive strength as well as the high work hardening behavior, respectively. Furthermore, it was found that adiabatic heating, which progressively becomes dominant at higher strain rates, decreases the transformation rate of retained austenite to martensite.

Independently of the strain rate, the material displayed a shear failure at an angle of 45° to the loading direction (Fig.3b). However, it was found that higher strain rates resulted in higher carbide fracture rates as well as carbide delamination at lower strains. It is assumed that this process, in combination with the impediment of strain accommodation processes [15], cause a premature sample failure at higher strain rates under compressive loading.

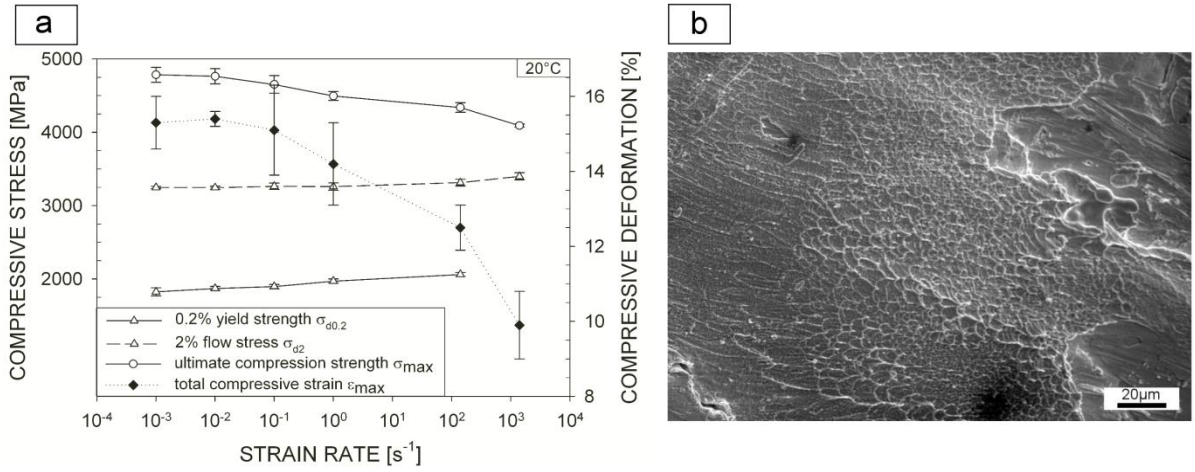

Fig.3: a) Mechanical properties as a function of strain rate after compressive loading; b) SEM image of a fractured surface displaying shearing dimples (sample deformed at $\dot{\varepsilon} = 1s^{-1}$).

Fracture toughness behavior

For the material investigated, fracture toughness K_{Ic} values at room temperature of 19.7±1.9MPa√m and at -40°C of 20.9±1.5MPa√m were determined. Due to the non-varying fracture toughness at -40°C, it is concluded that the lower shelf of K_{Ic} is already reached at room temperature. Fig.4 depicts SEM examinations of the fractured surfaces at both temperatures, showing transcrystalline cleavage fracture.

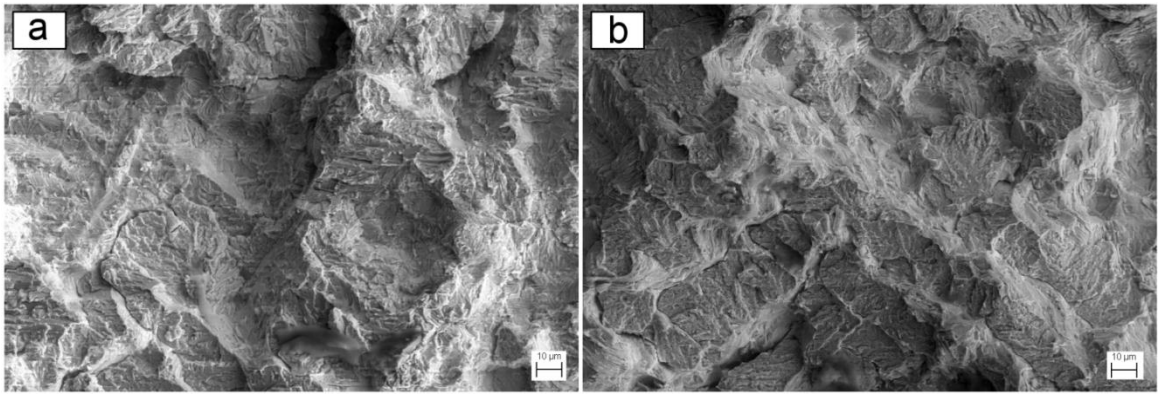

Fig.4: SEM examinations of the fracture surface under quasi-static conditions of $\dot{K}$=0.7 MPa√m/s at -40°C (a), and at room temperature (b).

A comparison of the determined fracture toughness at room temperature with literature data of tool steels revealed a relatively good fracture toughness behavior, as the K_{Ic} value is located in the upper part of the range of variation (Fig.5a).
In Fig.5b, a section of the fatigue precrack path is displayed. It becomes evident that the precrack did not necessarily follow the coherent ledeburitic carbide network. Furthermore, examinations revealed two facts. Firstly, fatigue precrack branching was observed, which is assumed to be a sign of inherent toughness. Secondly, the fact that the carbides broke but did not become extensively disconnected from the matrix points out that the boundary strength between the matrix and the eutectic carbides is relatively high.

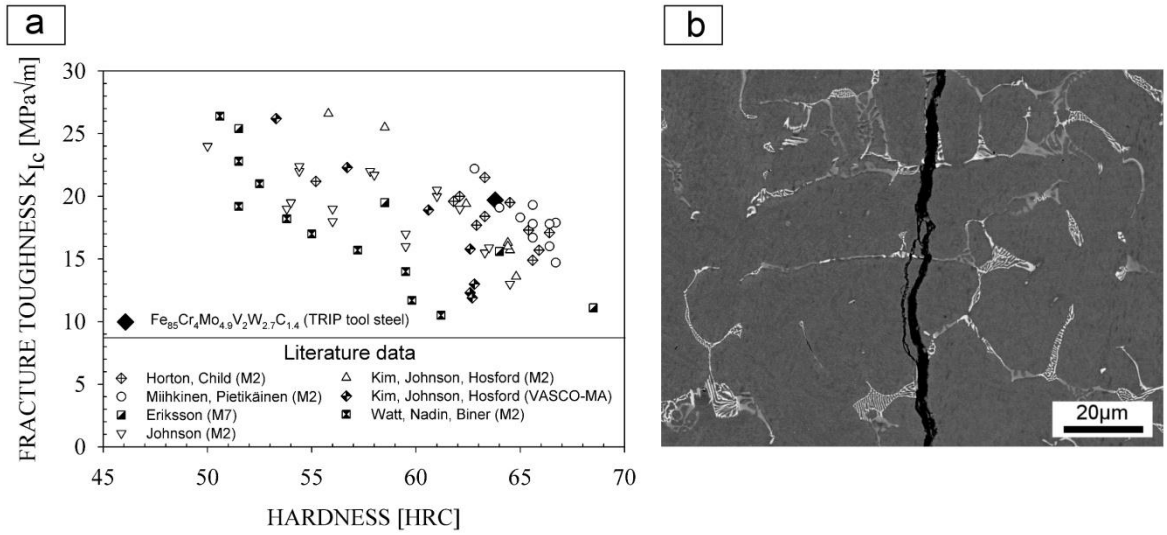

Fig.5: Comparison of fracture toughness values as a function of hardness for various tool steels (a), and path as well as branching of the fatigue precrack (b).

In Fig.6, the results of the examination of the influence of notch tip radius ρ on the notch fracture toughness K_A are displayed. A linear correlation between K_A and $\sqrt{\rho}$ up to a notch radius of 0.09mm was determined. At a notch radius of 0.035mm, the linear correlation breaks down. As a consequence, K_A at this particular notch radius is independent of $\sqrt{\rho}$ and thus identical to K_{Ic}. Based on the experimental findings, it is assumed that the critical notch tip radius ρ_c for the present alloy is approximately 90µm. As a result, the K_A value at a notch radius of 0.09mm represents a valid fracture toughness K_{Ic} value. The advantage of generating valid K_{Ic} values in sharply notched specimens is that the complicated and time-consuming precracking procedure might be avoided. Comparing the investigated material with M2 high-speed steel from literature data [16], high notch sensitivity becomes apparent. For technical applications, therefore, a design with high notch radii as well as precision machining is essential.
The results of the dynamic fracture toughness tests are displayed in Fig.6b. Increased rates of stress intensity $\dot{K}$ lead to lower dynamic fracture toughness K_{Id} values. In SEM examinations of the fractured surfaces, no differences between the K_{Ic} and K_{Id} specimens were obvious. Similarly to the illustrations in Fig.4, the K_{Id} samples exhibited entirely transcrystalline cleavage fracture.

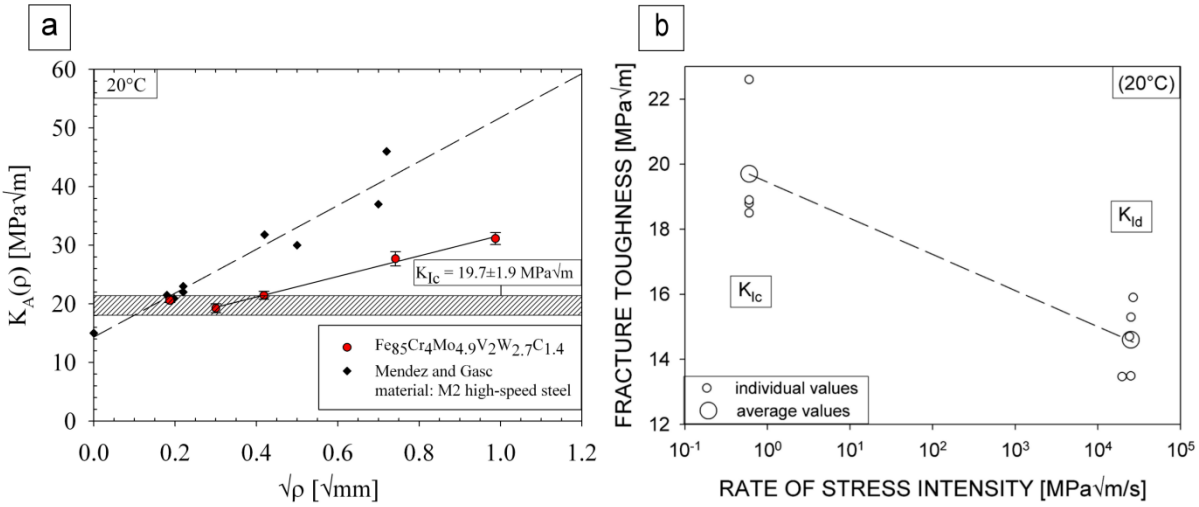

Fig.6: a) Notch fracture toughness K_A as a function of the square root of the notch radius √ρ for $Fe_{85}Cr_4Mo_{4.9}V_{2.1}W_{2.7}C_{1.4}$ steel as well as for M2 high speed steel [16]; b) Static (K_{Ic}) and dynamic (K_{Id}) fracture toughness values of $Fe_{85}Cr_4Mo_{4.9}V_{2.1}W_{2.7}C_{1.4}$ steel.

Summary

This study focused on the characterization of the microstructure, strain rate-dependent material and fracture toughness behavior of a high strength $Fe_{85}Cr_4Mo_{4.9}V_{2.1}W_{2.7}C_{1.4}$ steel. The following conclusions summarize the outcome of this research:

1. The microstructure consists of martensite, retained austenite and complex carbides.
2. High yield strength, flow stresses and ultimate compression strength values at a respectable deformation were measured. The material revealed a moderate strain rate sensitivity of the yield strength. Plastic deformation results in a strain-induced transformation of retained austenite to α'-martensite (the TRIP-effect).
3. Partitioning processes of the crystallites in combination with incrementally-formed martensitic boundaries result in smaller crystallite sizes and higher microstrains. These processes might be an explanation for the high work hardening behavior.
4. Fatigue precracking of this brittle material with an 8-point-bending device leads to stable crack propagation from a machined chevron-notch at a minimum-to-maximum stress ratio of R = -1.
5. In comparison to other tool steels the material possesses relatively high fracture toughness, while exhibiting high notch sensitivity. A critical notch tip radius ρ_c of approximately 0.09mm is assumed. Due to the fact that the lower shelf of K_{Ic} is already attained at room temperature, lower temperatures have no influence on K_{Ic}. In contrast, higher crack tip loading rates $\dot{K}$ resulted in lower dynamic fracture toughness values.

References

[1] H.D. Kunze, L.W. Meyer in: Metallurgical applications of shock-wave and high-strain rate phenomena, edited by L.E. Murr, K.P. Staudhammer, M.A. Meyers, Dekker, New York (1986), pp. 481-507.

[2] N.S. Brar, C. Hari Manoj Simha: J. Phys. IV Vol. 10 (2000), pp. Pr.9-611-Pr9-615.

[3] C.A.C. Imbert, H.J. Mc Queen: Mater Sci Eng A Vol. 313 (2001), pp. 88-103.

[4] S.A. Horton, H.C. Child: Met Tech Vol. 10 (1983), pp. 245-256.

[5] V. Leskovsek, B. Sustarsic, G. Jutrisa: J Mater Process Tech Vol. 178 (2006), pp. 328-334.

[6] P. Muro, S. Gimenez, I. Iturriza: Scripta Mater Vol. 46(5) (2002), pp. 369-373.

[7] A. Kokosza, J. Pacyna: Arch Mater Sci Eng Vol. 31(2) (2008), pp. 87-90.

[8] J. Blaha, E.A. Werner, W. Liebfahrt: Second International Conference on Processing Materials for Properties, 2000, San Francisco, S. 623-628.

[9] J. Pacyna, A. Mazur: Steel Res Vol. 57(11) (1986), pp. 577-585.

[10] A. Kulmburg, A. Schindler, H.P. Fauland, G. Hackl: HTM Vol. 49 (1994), pp. 31-39.

[11] ASTM E399-08: Standard test method for linear-elastic plane-strain fracture toughness K_{Ic} of metallic materials (2008).

[12] ISO 12108: Metallic materials - Fatigue testing - Fatigue crack growth method (2002).

[13] Y. Murakami: Stress intensity factors handbook Vol.1 (1987), Pergamon Press, Oxford.

[14] M. Rüssel, S. Martin, L. Krüger, W. Kreuzer: Accepted for publication in Metall Mater Trans A (2012).

[15] N. Hansen: Metall Mater Trans A Vol. 16 (1985), pp. 2167-2190.

[16] J. Mendez, C. Gasc: Int J Fracture Vol. 13 (1977), pp. 365-367.